Polymer 51 (2010) 5942–5951

Contents lists available at ScienceDirect

Polymer

journal homepage: www.elsevier.com/locate/polymer

Synthesis and characterization of dual stimuli-responsive block copolymers based on poly(*N*-isopropylacrylamide)-*b*-poly(pseudoamino acid)

Ren-Shen Lee*, Wen-Hsin Chen, Yi-Ting Huang

The Center of General Education, Chang Gung University, 259 Wen-Hwa 1st Road, Kwei-Shan, Tao-Yuan 333, Taiwan, ROC

ARTICLE INFO

Article history:
Received 10 July 2010
Received in revised form
23 September 2010
Accepted 2 October 2010
Available online 16 October 2010

Keywords:
Amphiphilic
Temperature/pH-sensitive
Block copolymer

ABSTRACT

The current study synthesized amphiphilic thermal/pH-sensitive block copolymers PNiPAAm-*b*-PHpr by condensation polymerization of *trans*-4-hydroxy-L-proline (Hpr) initiated from hydroxy-terminated poly(*N*-isopropylacrylamide) (PNiPAAm) as the macroinitiator in the presence of the catalyst, $SnOct_2$. ^1H NMR, FTIR, and gel permeation chromatography (GPC) characterized these copolymers. Their solutions showed reversible changes in optical properties: transparent below a lower critical solution temperature (LCST) and opaque above the LCST. The LCST values depended on the polymer composition and the media. With critical micelle concentrations (CMCs) in the range of 1.23–3.73 mg L^{-1}, the block copolymers formed micelles in the aqueous phase owing to their amphiphilic characteristics. Increased hydrophobic segment length or decreased hydrophilic segment length in an amphiphilic diblock copolymer produced lower CMC values. The current work proved the core-shell structure of micelles by ^1H NMR analyses of the micelles in D_2O. Transmission electron microscopy analyzed micelle morphology, showing a spherical core-shell structure. The micelles had an average size in the range of 170210 nm (blank), and 195280 nm (with drug). Observations showed high drug entrapment efficiency and drug-loading content for the drug micelles.

1. Introduction

In the last decade, various fields have focused considerable attention on stimuli-responsive polymers [1]. These polymers can be used in areas such as drug delivery, tissue engineering, biosensing, and separation processes due to their sensitivity to environmental changes [2–4]. Even though there are many stimuli, such as temperature, pH, light, and electric fields, more studies have focused on temperature- and/or pH-responsive materials for biomedical applications [5–7]. Recently, some double-hydrophilic copolymers capable of sensing both temperature and pH have been designed. Changing pH and/or temperature can alter their hydrophobic/hydrophilic properties [8–15]. Thermo- and pH-responsive polymers consisting of thermoresponsive polymeric units and acidic or basic polymer units, for example, poly((*N*,*N*-dimethylamino)ethyl methacrylate-*co*-ethylacrylamide) [16], poly(amidoamine)-poly(ethylene glycol)-poly(amidoamine) [17], poly(*N*-isopropylacrylamide)-poly(vinylphosphonic acid) [18], poly(α-*N*-substituted γ-glutamine)s [5], poly(L-glutamic acid)-poly(*N*-isopropylacrylamide) [19], poly((L-glutamic acid)-*co*-(γ-benzyl-L-glutamate)) [20], and poly(*N*-isopropylacrylamide)-poly(L-lysine) [21] were reported.

Some examples of functional polymers for biomedical use are pseudopoly(amino acid)s containing amino acid residues in the main chain. Pseudopoly(amino acid)s based on amino acids are expected to be nontoxic, biodegradable, and biocompatible because amino acids are naturally occurring compounds. Another advantage of using amino acids to prepare biologically functional biodegradable polymers is that amino acids are biologically active themselves. Pseudopoly(4-hydroxy-L-proline) (PHpr) can be dissolved in water directly at low pH. However, PHpr exhibits various degrees of hydrophobicity under basic conditions because the $-NH_2^+-$ groups are deprotonated and, hence, insoluble in water [22–24].

This study blocks hydrophobic segments of poly(*N*-benzyloxycarbonyl-4-hydroxy-L-proline) (PNZHpr) to the hydrophilic block of poly(*N*-isopropylacrylamide) (PNiPAAm) to form a core-shell nanoparticle with temperature/pH-sensitivity and biodegradability. Literature searches have not indicated that any previous research has investigated PNiPAAm-*b*-PNZHpr diblock copolymers. In our research, we choose 4-hydroxyproline (PHpr) to introduce functional groups on PNiPAAm because PHpr is a kind of amino acid needs must by human body and has the advantage of being nontoxic, biodegradable, biocompatible and fitted with pendant functional groups on the backbone which drugs or biologically active compounds can be covalently attached. This study predicts that polymeric micelles will dissociate into block copolymers when the hydrophobic segments

* Corresponding author. Tel.: +886 3 2118800x5054; fax: +886 3 2118700.
E-mail address: shen21@mail.cgu.edu.tw (R.-S. Lee).

0032-3861/$ – see front matter Crown Copyright © 2010 Published by Elsevier Ltd. All rights reserved.
doi:10.1016/j.polymer.2010.10.001

PNZHpr are degraded. The PNiPAAm block may compose a hydrophilic corona of the PNiPAAm-*b*-PNZHpr nanoparticles acting as a temperature sensitive component. The current study expected PNiPAAm-*b*-PNZHpr nanoparticles to form a core-shell type polymer that self-aggregates with a thermo-sensitive nanoparticle corona. For detailed investigation, this research synthesized PNiPAAm-*b*-PNZ(H)Hpr diblock copolymers with various PNiPAAm and PNZ(H)Hpr block lengths. Then, thermo/pH-sensitive PNiPAAm-*b*-PNZ(H)Hpr nanoparticles were prepared by a dialysis method to investigate their physicochemical characteristics and thermo/pH-sensitivities. Finally, the investigation examined the efficiency of PNiPAAm-*b*-PNZ(H)Hpr nanoparticles as drug carriers with the hydrophobic model drug, indomethacin.

2. Experimental

2.1. Materials

N-Isopropylacrylamide (NiPAAm), 2-mercaptoethanol (ME), benzoyl peroxide (BPO), and pyrene were purchased from the Aldrich Chemical Co. (Milwaukee, WI). *trans*-4-Hydroxy-*N*-benzyloxycarbonyl-L-proline (NZHpr) and indomethacin were purchased from the Fluka Chemical Co. (Buchs SGI, Switzerland). Stannous octoate ($SnOct_2$) was purchased from the Strem Chemical Co. (Newburyport, MA). Organic solvents such as tetrahydrofuran (THF), methanol, chloroform, *N*,*N*-dimethyl formamide (DMF) and *n*-hexane with a high pressure liquid chromatography (HPLC) grade were purchased from the Merck Chemical (Darmstad, Germany). Ultrapure water was obtained by purification with a Milli-Q Plus (Waters, Milford, MA).

2.2. Synthesis of PNiPAAm-b-PNZHpr

Block copolymers with different contents and compositions were synthesized according to the previously discussed method (Scheme 1) [25]. A hydroxy-terminated PNiPAAm precursor polymer was prepared by radical polymerization using BPO as an initiator and 2-hydroxyethanethiol as a chain transfer agent (CTA). For instance, *N*-isopropylacrylamide (4.2 g, 37.1 mmol), 2-hydroxyethanethiol (0.29 g, 3.71 mmol) and BPO (83.4 mg, 2 wt%) were dissolved in 15 mL of THF. The solution was degassed by bubbling with nitrogen for 20 min. The reaction mixture was refluxed under nitrogen for 24 h. Upon reflux completion, the product was precipitated out by adding diethyl ether. Using $SnOct_2$ as the catalyst, block copolymers of PNiPAAm-*b*-PNZHpr were synthesized by condensation polymerization of NZHpr with the hydroxy-terminated precursor in chlorobenzene. The precursor polymer and all monomers were dried in a vacuum oven before reaction. Then, the dried monomers and the precursor were charged into a flamed flask and nitrogen-purged several times to eliminate any moisture. The reaction mixture was refluxed at 132 °C for 24 h under nitrogen and used the Dean–Stark trap for water removal to reduce the homopolymerization. The product was concentrated under reduced pressure. Then, purification was performed by dissolving the polymer sample in chloroform and slowly adding into an excess of ether/hexane (1:1) mixture. The polymers were collected and dried *in vacuo* at 50 °C for 24 h. Table 1 lists the properties of the resultant block copolymers. Figs. 1(A) and 2(B) show the representative ^{1}H NMR and FTIR of PNiPAAm36-*b*-PNZHpr78.

2.3. Deprotection of PNiPAAm-b-PNZHpr

PNiPAAm-*b*-PHpr was prepared by deprotection of PNiPAAm-*b*-PNZHpr using HBr/CH_3CO_2H. As per the typical procedure, PNiPAAm-*b*-PNZHpr (1.04 g, 0.043 mmol) was dissolved in 6 mL of trifluoroacetic acid. Then, 4 equiv of 33% HBr/CH_3CO_2H with respect to the benzyl carbamate (Z) group was added and the solution was stirred for 1 h at room temperature. The solution was slowly poured into an excess of diethyl ether under vigorous stirring to precipitate the polymer. Then, the product was washed with diethyl ether 4 times. The polymer was isolated and dried at 50 °C. Figs. 1(C) and 2(C) show the representative ^{1}H NMR and FTIR of PNiPAAm36-*b*-PHpr81.

2.4. Characterization

^{1}H NMR spectra were recorded with a Bruker WB/DMX-500 spectrometer (Ettlingen, Germany) at 500 MHz with chloroform ($\delta = 7.24$ ppm) as an internal standard in chloroform-*d* ($CDCl_3$). IR spectra were measured on a Bruker TENSOR 27 Fourier transform infrared (FTIR) spectrophotometer (Bruker, Germany). Samples were either placed neatly on NaCl plates or pressed into KBr pellets. A GPC system determined the number and weight-average molecular weights (M_n and M_w, respectively) of the polymer. They were then carried out on a Jasco HPLC system equipped with a model PU-2031 refractive-index detector (Tokyo, Japan). Jordi Gel polydivinyl benzene (DVB) columns with pore sizes of 100, 500, and 1000 Å were used. Chloroform was used as the eluent at a flow rate of

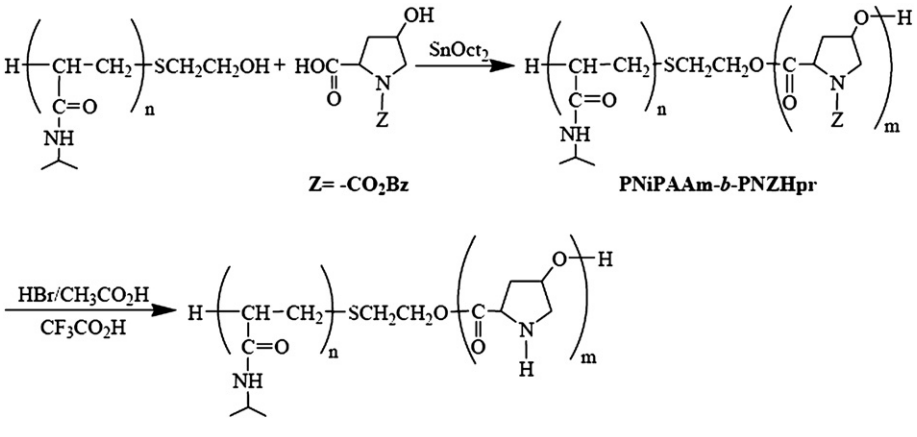

Scheme 1. Synthesis of PNiPAAm-*b*-PHpr block copolymer.

Table 1
Results of he block copolymerization of *N*-benzyloxycarbonyl-4-hydroxy-L-proline initiated with hydroxyl-terminated PNiPAAm[a].

Copolymer	[NZHpr]/[PNiPAAm] Molar ratio in feed	[NZHpr]/[PNiPAAm] Molar ratio[b]	$W_{PNiPAAm}$ (%)[c]	Yield (%)[d]	$M_{n,NMR}$[b]	$M_{n,th}$[d]	M_w/M_n[e]	LCST (°C)[f]	
								In DI water	In PBS (0.1 M)
PNiPAAm7-*b*-PNZHpr32	30/1	32/1	11	92	8261	7799	2.09	ND[g]	36[h]
PNiPAAm7-*b*-PNZHpr52	50/1	52/1	7	99	13714	12419	2.10	ND	38[h]
PNiPAAm7-*b*-PNZHpr62	70/1	62/1	6	98	15191	17039	1.58	ND	ND
PNiPAAm20-*b*-PNZHpr29	30/1	29/1	23	89	9503	9268	1.83	ND	35
PNiPAAm20-*b*-PNZHpr53	50/1	53/1	16	91	14581	13888	2.17	ND	38
PNiPAAm20-*b*-PNZHpr71	70/1	71/1	12	95	18739	18508	1.76	47	40
PNiPAAm36-*b*-PNZHpr78	70/1	78/1	19	93	22164	20316	1.60	46	39
PNiPAAm36-*b*-(PHpr34/PNZHpr44)	78/1	34/44/1	23	70	18152	12960	1.54	42	35
PNiPAAm36-*b*-PHpr81	78/1	81/1	44	98	13299	12960	–	ND	ND

[a] $M_{n,NMR}$ was 870 for PNiPAAm7, 2340 for PNiPAAm20 and 4152 for PNiPAAm36.
[b] Determined by ^{1}H NMR spectroscopy of PNiPAAm-*b*-PNZHpr.
[c] $W_{PNiPAAm}$: weight fraction of hydrophilic segment PNiPAAm.
[d] $M_{n,th} = M_{n,NMR} + M_{NZHpr} \times [M]/[I]$ (where $M_{n,NMR}$ is the number-average molecular weight of PNiPAAm, M_{NZHpr} is the molecular weight of NZHpr, $[M]$ is the monomer molarity concentration, and $[I]$ is the macroinitiator molarity concentration).
[e] Determined by GPC.
[f] LCST was determined by spectroscopically at 500 nm in 0.2 wt% aqueous polymer solution. The LCSTs were 47.6, 34.8, and 34.5 °C in DI water, and 41.3, 31.9, and 31.9 °C in PBS (0.1 MpH 7.4) for PNiPAAm7, PNiPAAm20, and PNiPAAm36, respectively.
[g] Abbreviation: ND = No detected.
[h] LCST was measured in 2 wt% solution.

0.5 mL min^{-1}. PEG standards with a low dispersity (Polymer Sciences) were used to generate a calibration curve. Data were recorded and manipulated with a Windows-based software package (Scientific Information Service). Pyrene fluorescence spectra were recorded on a Hitachi F-4500 spectrofluorometer (Japan). Square quartz cells of 1.0 cm × 1.0 cm were used. The detection wavelength (λ_{em}) was set at 390 nm for fluorescence excitation spectra.

2.5. Transmittance measurements

Optical transmittance of the aqueous polymer solution (2 mg mL^{-1}, 0.2 wt%) was measured at 500 nm with a UV–vis spectrometer (Jasco V-550, Japan) at various temperatures. Sample cells were thermostated with a temperature-controller (Jasco ETC-505T, Japan). Heating rate was 0.1 °C min^{-1}. LCST values of polymer solutions were determined at the temperature with half of the optical transmittance between below and above the transition.

2.6. Fluorescence measurements

Fluorescence measurements were carried out using pyrene as a probe to prove micelle formation [26]. Fluorescence spectra of pyrene in aqueous solution were recorded at room temperature on a fluorescence spectrophotometer. The sample solutions were prepared by first adding known amounts of pyrene in acetone to a series of flasks. After complete acetone evaporation, measured amounts of micelle solutions with various concentrations of PNiPAAm-*b*-PNZHpr ranging from 0.0183 to 9.38 mg L^{-1} were added to each flask and mixed by vortexing. In the final solutions, the pyrene concentration was 6.1 × 10^{-7} M. The flasks were allowed to stand overnight at room temperature to equilibrate the pyrene and the micelles. The emission wavelength was 390 nm for excitation spectra.

2.7. Preparation of polymeric micelles

Polymeric micelles of PNiPAAm-*b*-PNZHpr copolymers were prepared using the dialysis method [27]. Briefly, a solution of PNiPAAm-*b*-PNZHpr copolymer (30 mg) in DMF (5 mL) was placed in a dialysis bag (MWCO = 3500) and dialyzed against deionized (DI) water at ambient temperature for 24 h. The water was replaced at 2 h intervals.

2.8. Dynamic light-scattering measurements

The micelle size and size distribution of the thermo/pH-sensitive micelles were investigated by dynamic light scattering (DLS, Zetasizer nano ZS, Malvern, UK). DLS was equipped with an argon laser operating at 632.8 nm with a fixed scattering angle of 90° at 20 °C. Measurements were taken after the aqueous micellar solution (C = 0.3 g L^{-1}) was filtered with a microfilter with an average pore size of 0.2 μm (Advantec MFS, USA). The average size distribution of the aqueous micellar solution was determined based on CONTIN programs of Provencher and Hendrix [28].

2.9. Transmission electron microscope (TEM) measurements

Microscopic images of micelles were observed by TEM (JEM 1200-EXII, Tokyo, Japan). Drops of micelle solution (C = 0.3 g L^{-1}, without a stain agent) were placed on a carbon film coated copper grid, and then dried at room temperature. The observation was conducted at an accelerating voltage of 100 kV.

2.10. Drug-loading content and drug entrapment efficiency determinants

PNiPAAm-*b*-PNZHpr (50-fold CMC value) was dissolved in 6 mL of methylene chloride using oil-in-water solvent evaporation. This was followed by adding the anti-inflammatory drug indomethacin (IMC) in varying weight ratios to the polymer (0.1:1–2:1) serving as a model drug. The solution was added dropwise to 150 mL distilled water under vigorous stirring. Sonication for 60 min reduced droplet size at ambient temperature. The emulsion was stirred at ambient temperature overnight to evaporate the methylene chloride. The unloaded residue of IMC was removed by filtration using a Teflon filter (Whatman) with an average pore size of 0.45 μm. The micelles were obtained by vacuum drying. The addition of a ten-fold excess volume of DMF disrupted a weighed amount of micelle. Drug content was assayed spectrophotometrically at 320 nm using a Diode Array UV–vis spectrophotometer. Eqs. (1) and (2) calculate the drug-loading content and drug entrapment efficiency, respectively:

$$\text{Drug} - \text{loading content}\ (\%) = (\text{weight of drug in micelles}/\text{weight of micelles}) \times 100 \quad (1)$$

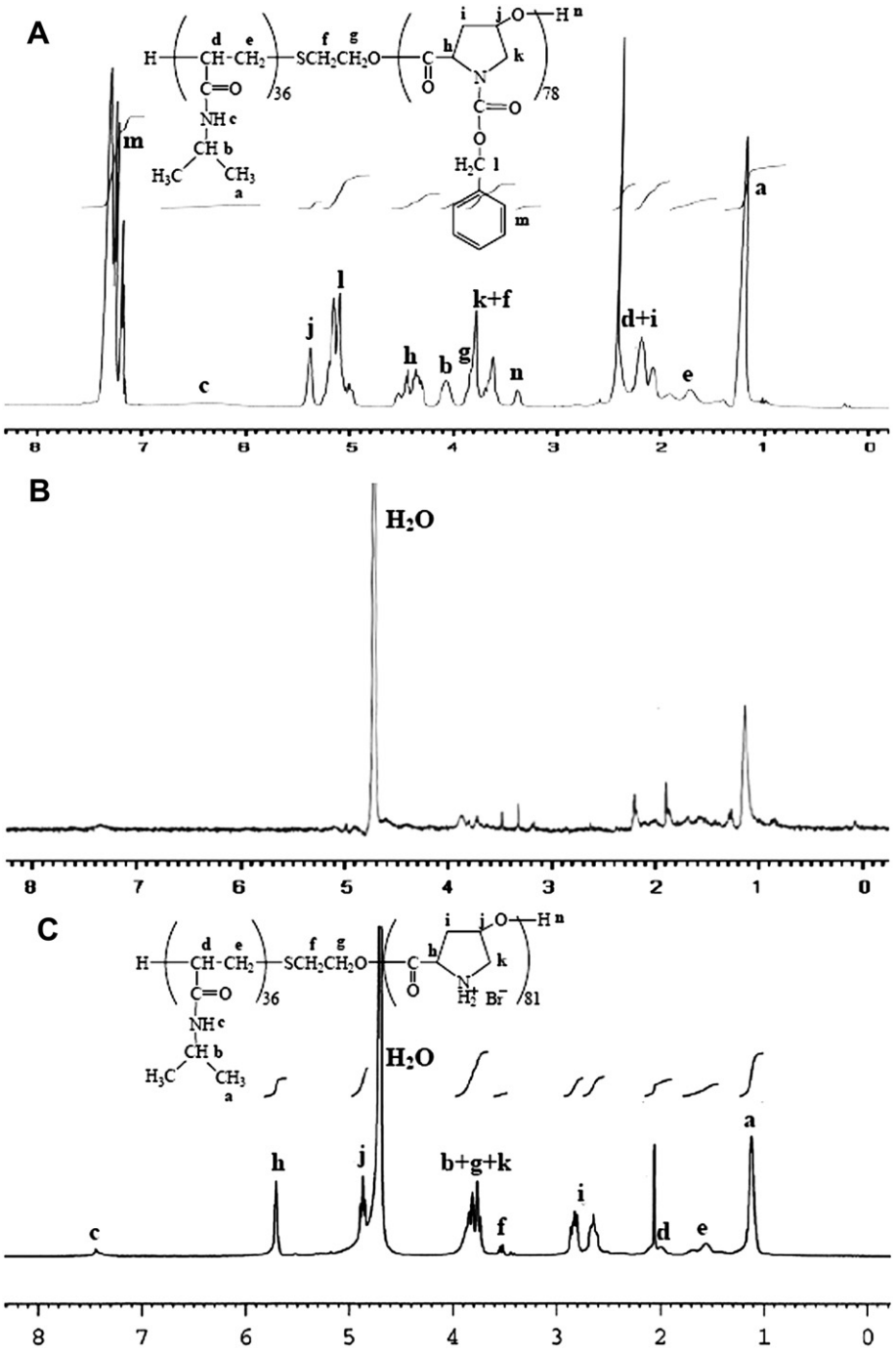

Fig. 1. Representative ^{1}H NMR spectra of (A) PNiPAAm36-*b*-PNZHpr78 in $CDCl_3$, (B) PNiPAAm36-*b*-PNZHpr78 micelle in D_2O, and (C) deprotected PNiPAAm36-*b*-PHpr81 in D_2O.

$$\text{Drug entrapment efficiency (\%)} = (\text{weight of drug in micelles} / \text{weight of drug fed initially}) \times 100 \quad (2)$$

2.11. In vitro drug release studies

The appropriate amounts of the IMC-loaded micelles (110.2 mg) were precisely weighted and suspended in 10 mL of PBS (0.1M, pH 7.4). The micellar solution was introduced into a dialysis membrane bag (molecular weight cutoff = 3500), and the bag was placed in 50 mL of PBS release media; the media was shaken (30 rpm) at 40 °C or 25 °C. At predetermined time intervals, 3-mL aliquots of the aqueous solution were withdrawn from the release media, and the same volume of a fresh buffer solution was added. The concentration of released IMC was monitored with a UV–vis spectrophotometer at a wavelength of 320 nm. The rate of controlled drug release was measured by the accumulatively released weight of IMC according to the calibration curve of IMC.

2.12. In vitro degradation

In vitro degradation of approximately 50 mg thin pellets (or micelle) of copolymer was performed in 5 mL of PBS (0.1M, pH 7.4)

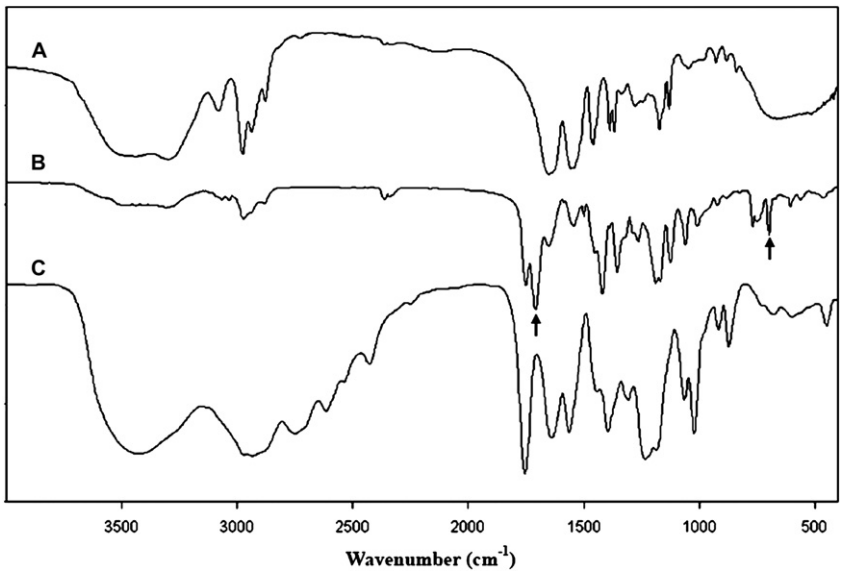

Fig. 2. IR spectra of (A) PNiPAAm36, (B) PNiPAAm36-*b*-PNZHpr78, and (C) PNiPAAm36-*b*-PHpr81.

at 37 °C. Additionally, the buffer solution was changed every 2 days. At time intervals, the specimen was removed, washed with distilled water, lyophilized, and weighed. The degree of degradation (%) was equal to $100(D_0-D)/D_0$, where D_0 was the weight of the copolymer before degradation and D was the weight of the copolymer after degradation for a specific period.

3. Results and discussion

3.1. Synthesis and characterization of PNiPAAm-b-PHpr block copolymers

The preparation of hydroxyl-terminated PNiPAAm has been reported for a long time. The molecular weight of PNiPAAm can be controlled by the ratio of NiPAAm to the chain transfer reagent. The $M_{n,NMR}$ of PNiPAAm was 870, 2340, and 4152 g mol^{-1} with $DP = 7$, 20, and 36, respectively. The polydispersity index (M_w/M_n) of PNiPAAm, determined from gel permeation chromatography (GPC), ranged from 1.19 to 1.40. These polymers were soluble in aqueous media at temperatures below their lower critical solution temperature (LCST). Findings showed that the LCSTs of these polymers depended on their molecular weights and the media. The LCST increased from 34.5 to 47.6 °C in DI water. Furthermore, the LCST increased from 31.9 to 41.3 °C in PBS when the molecular weight of PNiPAAm decreased from 4152 to 870 g mol^{-1}. The PNiPAAm polymers with lower molecular weights demonstrated higher LCST values. This was considered a result of hydrating contributions from polar terminal hydrophilic hydroxyl groups in the polymers. Larger end group contributions were expected for PNiPAAm with lower molecular weights. The LCSTs of PNiPAAm in PBS were lower than that in DI water. This is due to the increased ionic strength of PBS. Scheme 1 illustrates the synthesis of amphiphilic PNiPAAm-*b*-PHpr diblock copolymers. In the presence of the catalyst, $SnOct_2$ (1.5 wt %), this study used the PNiPAAm hydroxyl group as the initiation site for condensation polymerization of NZHpr in chlorobenzene at reflux for 24 h. Copolymers with different compositions were prepared by changing the monomer NZHpr feed ratio with the fixed macroinitiator. Table 1 compiles the results of polymerization. The yields between 89 and 99% were high. The $M_{n,NMR}$ of the block copolymers obtained from polymerization of NZHpr in the existence of PNiPAAm increased with the increase of NZHpr molar ratios to PNiPAAm in the feed. The molar ratios of NZHpr to PNiPAAm7 in the feed increased from 30 to 70 and the $M_{n,NMR}$ of the copolymer increased from 8261 to 15191 g mol^{-1} when using the PNiPAAm7 as the macroinitiator. The polydispersity index (M_w/M_n) of PNiPAAm7-*b*-PNZHpr, determined from gel permeation chromatography (GPC), ranged from 1.58 to 2.10. Similarly, when the PNiPAAm20 and PNiPAAm36 were used as macroinitiators, the $M_{n,NMR}$ of the block copolymers increased with the increase of NZHpr molar ratios to PNiPAAm in the feed. The molar ratio of block copolymers compositions was analyzed by ^{1}H NMR. The amounts of monomer incorporated into the copolymer were calculated from comparing the integral area of resonance peaks of the benzylic protons ($\delta = 5.11$ ppm) of PNZHpr with the resonance peaks of dimethyl protons ($\delta = 1.21$ ppm) of PNiPAAm. Polymerization of the monomers was in good agreement with the corresponding feeds from ^{1}H NMR analysis. Fig. 1(A) shows the typical ^{1}H NMR spectrum of the block copolymer PNiPAAm-*b*-PNZHpr. This study assigned typical signals to the corresponding hydrogen atoms of the copolymers. Observations showed typical signals of the PNiPAAm blocks at $\delta = 4.08$ ppm (H_b, $-CH(CH_3)_2$), 1.61–2.28 ppm (H_d, H_e, $-CH-$ and $-CH_2-$), and 1.21 ppm (Ha, $-CH(CH_3)_2$). Characteristic signals of the PNZHpr blocks were exhibited at $\delta = 7.39$–7.18 ppm (H_m, the protons of aromatic), 5.41–4.95 ppm (H_j, the methine proton and H_l, the benzylic protons), 4.58–4.26 ppm (H_h, the methine proton), 3.86–3.58 ppm (H_k, the methylene protons), and 2.29–2.01 ppm (H_i, the methylene protons). Fig. 2(B) shows the FTIR spectrum of the PNiPAAm36-*b*-PNZHpr78, in which the characteristic band at about 1749 cm^{-1} (νcarbonyl of ester), and 1705 cm^{-1} (νcarbonyl of urethane) are associated with PNZHpr.

The benzyloxycarbonyl protective groups of PNiPAAm-*b*-PNZHpr could only be partially removed by catalytic hydrogenolysis over Pd/C (10%) in THF/CH_3OH. Although PNiPAAm36-*b*-PNZHpr70 was performed under 2.0atm H_2 at 50 °C for 48 h, only 44% the benzyloxycarbonyl was removed. This was due to the poisoning of the catalyst by sulfur atoms in ME, a chain transfer agent. However, the double-hydrophilic copolymer PNiPAAm-*b*-PHpr was achieved after quantitative removal of the benzyl group from the PNZHpr block in PNiPAAm-*b*-PNZHpr with HBr/glacial acetic acid. Fig. 1(A) and (c) illustrates this point. The signals from the benzyl groups in PNiPAAm-*b*-PNZHpr at $\delta = 5.11$ and 7.29 ppm (Fig. 1(A)) disappeared completely upon deprotection (Fig. 1(C)). Fig. 2(B) and (c) illustrates

the same result in the FT-IR spectra. The absorption bands at 1705 cm^{-1} (νcarbonyl of urethane) and 698 cm^{-1} (νC—H out-of-plane bending of aromatic) disappeared completely upon deprotection.

3.2. LCST behavior

PNiPAAm is one of the most widely investigated thermo-sensitive polymers with highly extended coil to globule transition upon heating. The transition results in the precipitation of the sol to gel transformation of PNiPAAm or related copolymers. This work characterizes LCST behaviors of PNiPAAm-*b*-PNZ(H)Hpr copolymers solutions by measuring their cloud points. The LCSTs were determined at a temperature with half of the optical transmittance change between below and above the transition. Table 1 summarizes the results. The LCST values of PNiPAAm-*b*-PNZHpr copolymer solutions in DI water were higher than in PBS. Fig. 3(A) shows the transmittance changes in PNiPAAm36-*b*-PNZHpr78 in DI water and PBS solution. It was found that the cloud points and phase-transition curves of copolymer solutions shifted to a higher temperature and became broader in DI water solutions. Findings showed that the LCSTs of PNiPAAm-*b*-PNZHpr copolymers were higher than that of homo-PNiPAAm when the longer PNiPAAm (PNiPAAm20 and PNiPAAm36) was used. The LCST values increased when the length of PNZHpr block increased for the PNiPAAm20-*b*-PNZHpr series of copolymers. However, due to the easy solubility of PNiPAAm7-*b*-PNZHPr series of copolymers in DI water and PBS solution, no transition behaviors were observed when the shorter PNiPAAm (PNiPAAm7, 0.2 wt%) was used. But, as the concentration increased to 2 wt% in PBS, the LCSTs of PNiPAAm7-*b*-PNZHPr32 and PNiPAAm7-*b*-PNZHPr52 (lower than PNiPAAm7) were observed because the aggregation appeared when the temperature above the LCST. These outcomes indicate that hydrophilicity of the PNiPAAm block significantly affects the transition temperature of the corresponding copolymer.

Fig. 3(B) shows the transmittance changes in PNiPAAm-*b*-PHPr with different composition at different temperatures. It was found that the cloud points of the copolymer solutions shifted to a higher temperature at pH 7.4 with increasing PHpr content. The LCST increased from 33.7 to 50.5 °C when the weight fraction of PHpr (W_{PHpr}) increased from 58 to 89% in the PNiPAAm-*b*-PHPr copolymers. Furthermore, when the PHpr block was long enough, the transition was very weak even at a higher temperature range. The lowest transmittance for PNiPAAm17-*b*-PHpr24 was much higher than that of PNiPAAm7-*b*-PHpr62, which reached 60%. It can be anticipated that the LCST behavior of copolymers can be lost even as the length of the PHpr block increases. This suggests that the hydrophilicity of the PHpr block significantly affects the solution behavior of the corresponding copolymer. The temperature is higher than the LCST of PNiPAAm (32 °C) because soluble PHpr blocks enhance the hydrophilic property of the copolymer.

Fig. 4 shows the temperature-dependent phase-transition curves of the 0.2 wt% partially deprotected PNiPAAm36-*b*-(PHpr34/

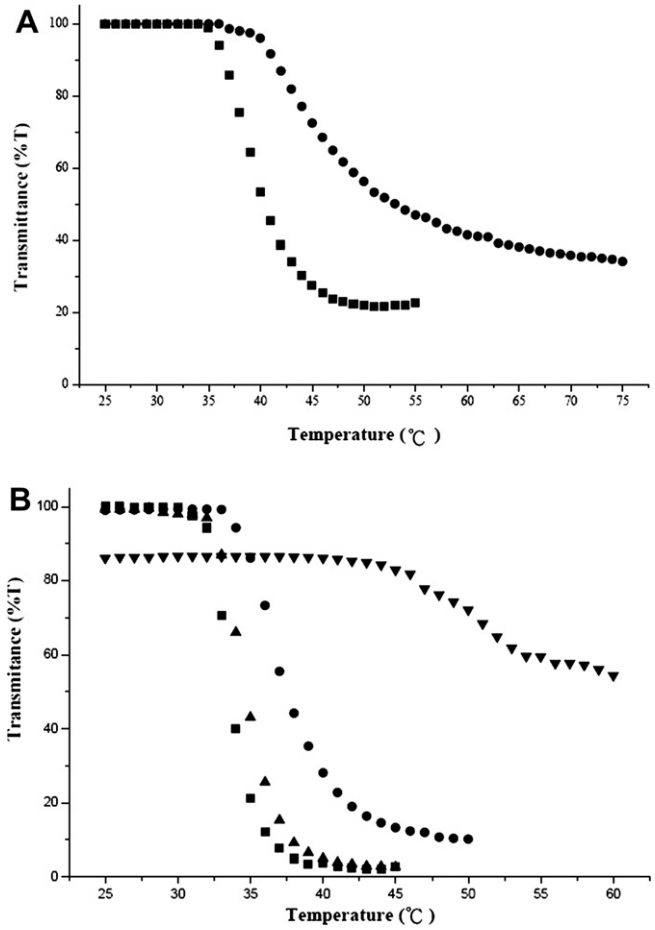

Fig. 3. Phase-transition curves of (A) PNiPAAm36-*b*-PNZHpr78 (0.2 wt%) in DI water (●), and in PBS (0.1M, pH 7.4) (■), (B) deprotected PNiPAAm-*b*-PHpr with the molar composition of PNiPAAm/PHpr : 17/24 (■), 36/81 (▲), 17/58 (●), 7/62 (▼) in PBS (0.1M, pH 7.4) at $\lambda = 500$ nm.

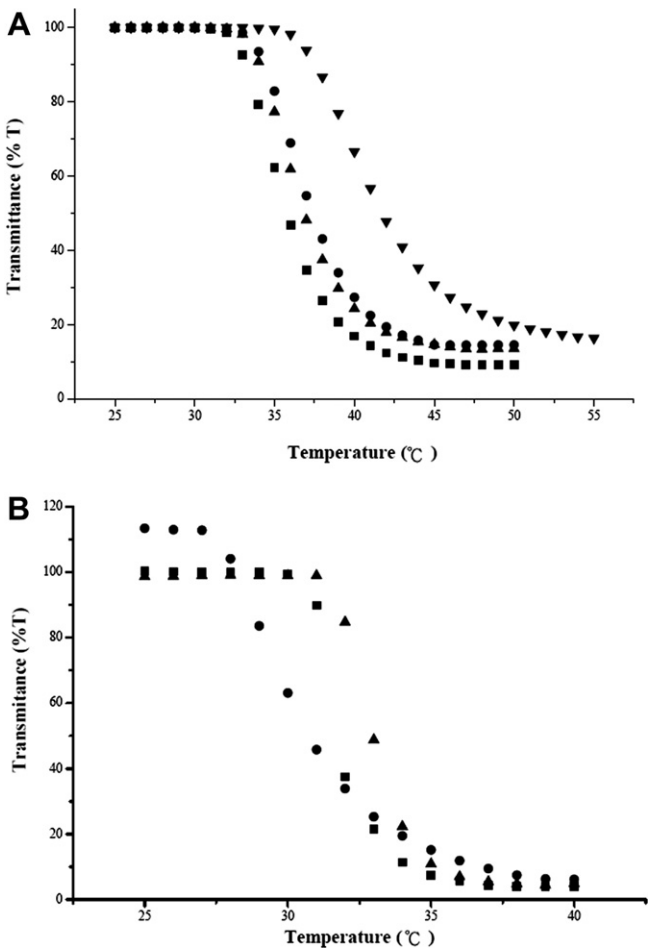

Fig. 4. Effect of pH on the phase-transition temperature of (A) PNiPAAm36-*b*-(PHpr34/PNZHpr44) (0.2 wt%) in PBS solution at pH 8.2 (■), 6.2 (▲), 4.2 (●), and 2.2 (▼), (B) PNiPAAm36-*b*-PHpr81 (0.2 wt%) in PBS at pH 10.0 (●), 7.4 (▲), and 4.0 (■).

PNZHpr44) and fully deprotected PNiPAAm36-*b*-PHpr81 PBS solutions at different pHs. For PNiPAAm36-*b*-(PHpr34/PNZHpr44), as the pH decreases from 8.2 to 4.2, the copolymer shows similar phase-transition curves, and the LCSTs only slightly increase (Fig. 4(A)). The curve exhibits a broader transformation when the pH is lowered to 2.2 and the LCST markedly increases because PHpr is highly protonated in an acidic condition, resulting in a more hydrophilic character. However, for PNiPAAm36-*b*-PHpr81, the LCSTs at either pH 10 (30.2 °C) or 4.0 (31.7 °C) are lower than at pH 7.4 (32.9 °C), suggesting the hydrophilicity no enhanced at pH 10 or 4.0 (Fig. 4(B)).

3.3. Micelles of block copolymers

The amphiphilic nature of block copolymers, consisting of hydrophilic PNiPAAm and hydrophobic PNZHpr blocks, provides an opportunity to form micelles in water. This study investigated the characteristics of block copolymer micelles in an aqueous phase by fluorescence techniques. A fluorescence technique, using pyrene as a probe, determined critical micelle concentrations (CMCs) of the block copolymers in an aqueous phase [29].

Fig. 5 shows the excitation spectra of pyrene in the PNiPAAm-*b*-PNZHpr solution at various concentrations. Findings indicate that fluorescence intensity increases with an increase in PNiPAAm-*b*-PNZHpr concentration. To determine CMC values of the PNiPAAm-*b*-PNZHpr block copolymers, this work utilized the characteristic pyrene excitation spectra, a red shift of the (0,0) band from 334 to 339 nm upon pyrene partition into a micellar hydrophobic core. Fig. 6 shows the intensity ratios (I_{339}/I_{334}) of pyrene excitation spectra versus the logarithm of PNiPAAm-*b*-PNZHpr copolymer concentrations. This study determined the CMC from intersecting straight-line segments lying on a nearly horizontal line, drawn through the points at the lowest polymer concentrations, with that going through the points on the rapidly rising part of the plot. Table 2 shows CMC values of block copolymers dependent on block composition. CMC values of the copolymers PNiPAAm-*b*-PNZHpr decrease with increasing hydrophobic PNZHpr chain length at the fixed length of the hydrophilic block. The CMC values decreased from 1.71 to 1.23 mg L^{-1} and from 3.22 to 2.23 mg L^{-1} for PNiPAAm7-*b*-PNZHpr, and PNiPAAm20-*b*-PNZHpr series copolymers, respectively. The CMC values were much lower than those of low-molecular-weight surfactants and comparable to those of other polymeric amphiphilies [30]. Low CMC values for PNiPAAm-*b*-PNZHpr copolymers indicate a very strong tendency of the diblock

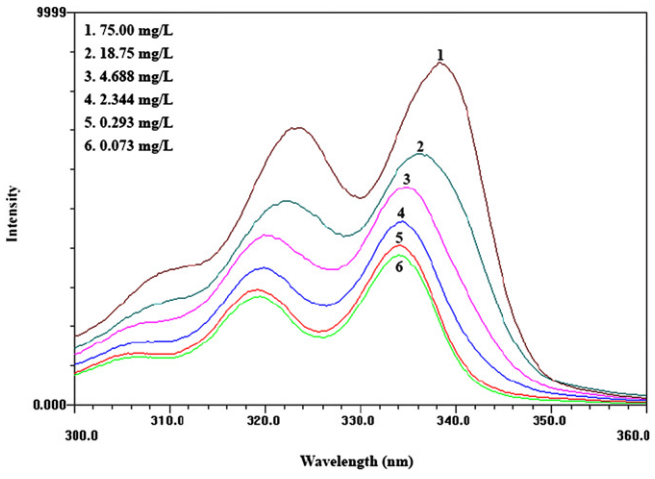

Fig. 5. Excitation spectra of the PNiPAAm20-*b*-PNZHpr29 copolymer monitored at $\lambda_{em} = 390$ nm.

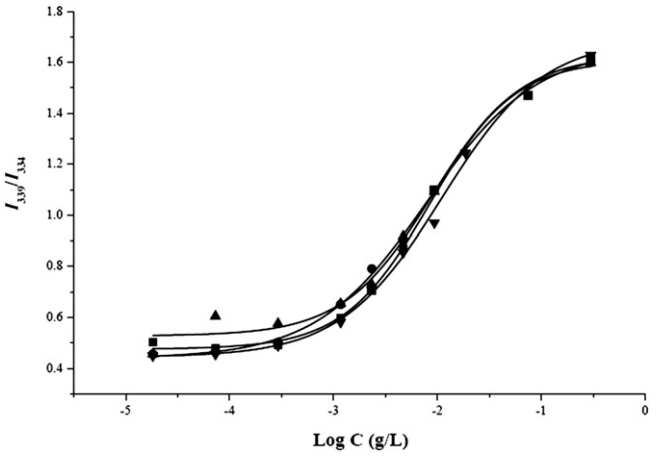

Fig. 6. Plot of I_{336}/I_{334} intensity ratio (from pyrene excitation spectra ; pyrene concentration = 6.1×10^{-7}) versus the logarithm of concentration (log *C*) for (●) PNiPAAm7-*b*-PNZHpr32, (▲) PNiPAAm7-*b*-PNZHpr52, (■) PNiPAAm7-*b*-PNZHpr62, (▼) PNiPAAm20-*b*-PNZHpr29 diblock copolymer (λ_{em} = 390 nm).

copolymers toward micelle formation in aqueous solution. An increased length of the hydrophilic (PNiPAAm) segment exhibits increased CMC values. The mean hydrodynamic diameters of micelles, measured by DLS, were in the range of 175–210 nm (Table 2). Fixing the concentration at 50-fold CMC (50 × CMC) value, the mean diameter of micelles increases with an increase in the length of hydrophobic segments. These facts indicate that micelle size depends on polymer composition (i.e. the length of the hydrophilic or hydrophobic segment in the chain). Fig. 7 also shows the micelle morphology of PNiPAAm20-*b*-PNZHpr53. The images confirmed that the copolymers form spherical core-shell shapes. The size was in agreement with the size previously determined by DLS. The amphiphilic block copolymer can self-aggregate to form nanoparticles consisting of a hydrophobic core and a hydrophilic shell in aqueous milieus. The formation of the hydrophobic PNZHpr domain can be confirmed by ^{1}H NMR spectra with $CDCl_3$ and D_2O as locking solvents for PNiPAAm-*b*-PNZHpr block copolymers. Fig. 1 (A) demonstrates that the complete structural resolution of each blocks was observed in $CDCl_3$, a nonselective solvent for PNiPAAm and PNZHpr blocks. However, in D_2O, only the PNiPAAm signals were detected, which mainly originate from the selective solvation of the exterior hydrophilic PNiPAAm shell through hydrogen bond formation with D_2O (Fig. 1(B)). The results revealed that the PNZHpr blocks in PNiPAAm-*b*-PNZHpr block copolymers form a hydrophobic domain in the nanoparticles and remain in a solid and/or semi-solid state. This results in the disappearance of the PNZHpr characteristic peaks in D_2O. Similar trends of ^{1}H NMR spectra are consistent with other amphiphilic block copolymer systems [31]. The Zeta potentials in the range of −1.8~−29 mv demonstrate the resultant micelles are instable to moderate stable. The Zeta potential is negative because due to the lone-pair electrons in PNiPAAm blocks.

3.4. Evaluation of drug-loading content and drug entrapment efficiency

This research measured the drug-loading content and entrapment efficiency of polymeric micelles fabricated by a dialysis method with various IMC-to-polymer feed ratios. IMC had a maximum absorption peak at 320 nm, which was proportional to concentration. The amount of loaded IMC was determined by absorbance at 320 nm after eliminating the unloaded precipitates

Table 2
Properties of IMC-loaded PNiPAAm-*b*-PNZ(H)Hpr micelles.

Copolymer	CMC (mg/L)	Feed weight ratio IMC/polymer	Drug entrapment efficiency (%)	Drug loading content (%)	Blank micelle (without IMC)		Drug loading micelle (with IMC)	
					Micelle size (nm)	Zeta potential (mv)	Micelle size (nm)	Zeta potential (mv)
PNiPAAm36-*b*-PNZHpr78	3.33	2/1	98.2	65.5	182.9 ± 2.4	−1.8	235.3 ± 15.2	−7.2
		1/1	86.9	43.5				
		1/5	75.9	12.7				
		1/10	74.0	6.72				
PNiPAAm7-*b*-PNZHpr32	1.71	1/1	96.3	48.2	177.2 ± 1.8	−18.7	207.0 ± 3.8	−12.5
PNiPAAm7-*b*-PNZHpr52	1.25	1/1	93.5	46.5	195.4 ± 0.6	−29.0	275.9 ± 4.6	−18.6
PNiPAAm7-*b*-PNZHpr62	1.23	1/1	54.6	27.3	202.8 ± 2.1	−17.6	194.7 ± 2.4	−26.2
PNiPAAm20-*b*-PNZHpr29	3.22	1/1	76.6	35.4	187.8 ± 2.1	−15.0	210.2 ± 18.2	−15.8
PNiPAAm20-*b*-PNZHpr53	2.46	1/1	74.9	32.4	190.5 ± 6.2	−26.9	237.4 ± 6.1	−16.8
PNiPAAm20-*b*-PNZHpr71	2.23	1/1	70.8	32.1	202.4 ± 5.2	−15.3		
PNiPAAm36-*b*-(PHpr34/PNZHpr44)	3.73	1/1	72.6	36.3	208.0 ± 41.4		230.0 ± 51.9	

of IMC. Table 2 shows the calculated drug-loading content and entrapment efficiency values. The amount of IMC introduced into the micelle was controlled by the weight ratio between the drug and the polymer. For example, in the PNiPAAm36-*b*-PNZHpr78 series, drug entrapment efficiency and drug-loading content increased when the drug to polymer weight ratio increased. The drug-loading content and entrapment efficiency showed a general increasing trend in these efficiencies (up to 48.2%, and 96.3%) with PNZHpr block length decrement at the constant feed weight ratio (1:1). Observations showed a similar increased tendency in drug-loading content and entrapment efficiency for PNiPAAm20-*b*-PNZHpr copolymers with different lengths of PNZHpr. These values strongly relate to the interaction parameters between the hydrophobic segment of the micelle and the drug. When hydrophilic segment length increased, a hydrophobic block of approximately the same length showed a decreased drug-loading content and entrapment efficiency. The drug-loading efficiency and drug content of the block copolymers with longer PNiPAAm blocks are lower than the block copolymers with short PNiPAAm blocks. This is may be due to that the micelles prepared from the block copolymers with longer PNiPAAm blocks are less stable. During drug loading, the PNiPAAm-*b*-PNZHpr block copolymers showed excellent characteristics as drug carriers due to their high drug-loading content and efficiency. The micelle size and Zeta potential of the drug loaded micelles were shown in Table 2. The micelle sizes of drug loaded almost larger than the blank were observed. Effect of pH on the drug-loading content and entrapment efficiency of PNiPAAm36-*b*-PHpr81 with weight ratio IMC/polymer 1:1 at room temperature was also investigated. The results are shown in Fig. 8. At pH 10, the drug-loading content and entrapment efficiency of PNiPAAm36-*b*-PHpr81 are higher than at pH 4.0 or 6.0. This is due to have larger hydrophobic interaction of PNiPAAm36-*b*-PHpr81 with IMC at pH 10.

3.5. In vitro release of IMC

Hydrophobic drugs could be loaded into the micelles due to the hydrophobic core of the micelles. Indomethacin, an anti-inflammatory drug with a very low solubility in water, was used as a model drug. The IMC release from PNiPAAm36-*b*-PNZHpr78 micelles was examined in PBS solution and release data are shown in Fig. 9. The profiles of drug release showed great change upon temperature alteration. A slow release was observed due to the more stable of micelles when the temperature was 25 °C (below the cloud point temperature). However, when the release temperature was increased to be 40 °C, drug release was much more accelerated due to the temperature induced structure change of the micelles. With respect to different release rates at two different temperatures (25 and 40 °C), the accelerated drug release was reasonable. The cloud point temperature of the micelles was 39 °C. When the temperature increased to 40 °C (or approximately the cloud point temperature), the hydrophilicity of the micellar shell, comprised of PNiPAAm chains, was weakened, resulting in the partial destruction of the micelles. Due to the partially destroyed micellar structure at 40 °C, the loaded drug was released more quickly in comparison with drug release at 25 °C. IMC releases of the PNiPAAm36-*b*-PNZHpr78 micelles are compared with the deprotected PNiPAAm36-*b*-PHpr81 micelles at 40 °C in PBS (0.1 M, pH 7.4). The accumulatively drug released of PNiPAAm36-*b*-PHpr81 micelles was slower than PNiPAAm36-*b*-PNZHpr78 micelles. This could be ascribed to the reason that the PHpr blocks have stronger intermolecular interactions with IMC *via* the hydrogen bonding.

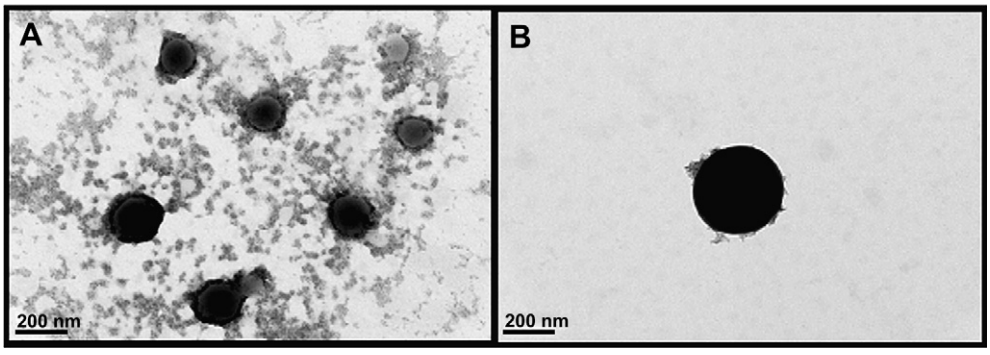

Fig. 7. TEM photograph of the micelles formed by PNiPAAm20-*b*-PNZHpr53 (A) blank, and (B) with drug.

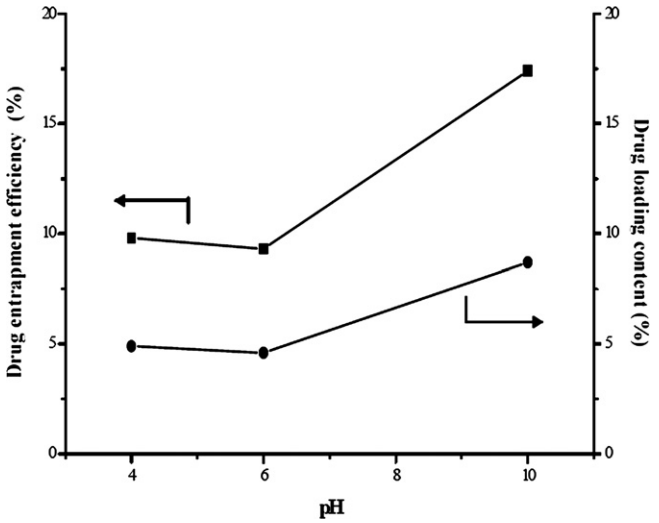

Fig. 8. Effect of pH on the drug-loading content and entrapment efficiency of PNiPAAm36-*b*-PHpr81 with weight ratio IMC/polymer 1:1 at room temperature.

3.6. Preliminary in vitro degradation study

The *in vitro* degradation of the PNiPAAm-*b*-PNZHpr, and deprotected PNiPAAm-*b*-PHpr were evaluated from the sample weight loss in the film (or micelle) as a model of biodegradation. Fig. 10(A) portrays the degradation profiles of PNiPAAm7-*b*-PNZHpr32, PNiPAAm20-*b*-PNiPAAm53 and PNiPAAm20-*b*-PNZHpr29 with $W_{PNiPAAm}$ of 11, 16, and 23%, respectively, at 37 °C under physiological conditions (pH 7.4). The results indicated that the weight loss of PNiPAAm20-*b*-PNZHpr29 was the most rapid with up to 15% weight loss after immersion for 30 days. The easier degradation of PNiPAAm20-*b*-PNZHpr29 was due to the higher $W_{PNiPAAm}$. Increased PNiPAAm contents in the copolymers increased their hydrophilicity and, thus, resulted in larger weight losses. The degradation profiles of deprotected PNiPAAm-*b*-PHpr copolymers with the composition [NiPAAm]/[Hpr]: 17/32, and 17/58 are shown in Fig. 10(B). In the thin-film, the weight losses of PNiPAAm-*b*-PHpr are rapidly up to 60% after immersion for first day. The weight loss of the deprotected PNiPAAm-*b*-PHpr is faster than the protected PNiPAAm-*b*-PNZHpr. The degradation of the PNiPAAm17-*b*-PHpr58 with longer Hpr blocks is easier than the PNiPAAm17-*b*-PHpr32. This is due to the PNiPAAm-*b*-PHpr with longer Hpr blocks more soluble in the aqueous solution. However, the weight loss of the PNiPAAm-*b*-PHpr micelle is very small, slower than the PNiPAAm-*b*-PHpr and PNiPAAm-*b*-PNZHpr pellets. This is ascribed to the reason that the degradable PHpr blocks were incorporated into the core of micelle.

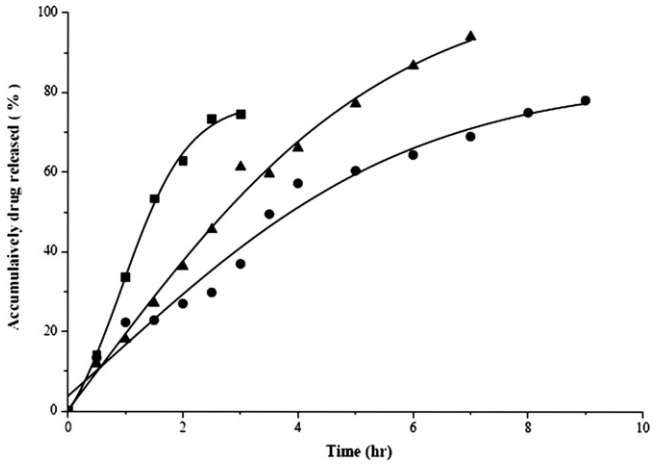

Fig. 9. IMC release of thermo-sensitive PNiPAAm36-*b*-PNZHpr78 micelles at 40 °C (■) and 25 °C (▼), and deprotected PNiPAAm36-*b*-PHpr81 micelles at 40 °C (▲) in PBS (0.1 M, pH 7.4) solution.

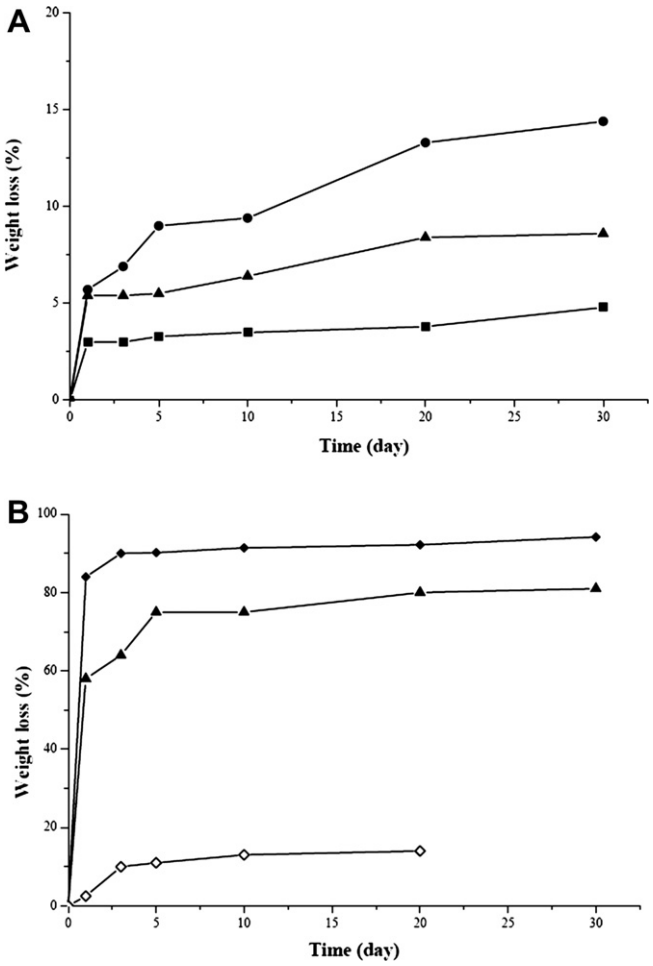

Fig. 10. Weight loss of (A) the thin pellets PNiPAAm-*b*-PNZHpr copolymers with the composition [NiPAAm]/[NZHpr] = 7/32 (▲), 20/29 (●), and 20/53 (■), (B) the thin pellets (or micelle) of PNiPAAm-*b*-PHpr copolymers with the composition [NiPAAm]/[Hpr] = 17/32 (▼: pellet), and 17/58 (◆: pellet, ◇: micelle)treated in 0.1M PBS (pH 7.4) at 37 °C.

4. Conclusion

This study successfully synthesized thermal/pH-sensitive block copolymers PNiPAAm-*b*-PNZ(H)Hpr by condensation polymerization using the hydroxy-terminated PNiPAAm as the macroinitiator. The LCST values of PNiPAAm-*b*-PNZ(H)Hpr copolymers depend on the molecular weight and media. The copolymers form micelles in aqueous solution, with the CMC dependent on polymer composition. Increased length of the hydrophobic segment or decreased length of the hydrophilic segment in an amphiphilic diblock copolymer produces lower CMC values. The DLS experiment shows that the micelles have an average size in the range 170210 nm (blank), and 195280 nm (with drug). The micelle morphology exhibits a spherical shape. Drug entrapment efficiency and drug-loading content decreased with increased length of the hydrophobic block.

Acknowledgements

This research was supported by grants from the National Science Council (NSC 99-2221-E-182-002) and ChangGung University (BMRP 123).

References

[1] Gil ES, Hudson SM. Prog Polym Sci 2004;29:1173–222.
[2] Bae YS, Fukushina S, Harada A, Kataoka K. Angew Chem Int Ed 2003;42:4640–3.
[3] Nitschke M, Gramm S, Gotze T, Valtink M, Drichel J, Voit B, et al. J Biomed Mater Res 2007;80a:1003–10.
[4] Reppy MA, Pindzola BA. Chem Commun; 2007:4317–8.
[5] Tachibana Y, Kurisawa M, Uyama H, Kobayashi S. Biomacromolecules 2003;4:1132–4.
[6] Liu XM, Wang LS. Biomaterials 2004;25:1929–36.
[7] Cai YL, Tang YQ, Armes SP. Macromolecules 2004;37:9728–37.
[8] Zhao C, Zhuang X, He P, Xiao C, He C, Sun J, et al. Polymer 2009;50:4308–16.
[9] Chang C, Wei H, Feng J, Wang ZC, Wu XJ, Wu DQ, et al. Macromolecules 2009;42:4838–44.
[10] Yin X, Stöver HDH. Macromolecules 2002;35:10181–718.
[11] Weber C, Becer CR, Guenther W, Hoogenboom R, Schubert US. Macromolecules 2010;43:160–7.
[12] Zhao Y, Su H, Fang L, Tan T. Polymer 2005;46:5368–76.
[13] Lo CL, Lin KM, Hsiue GH. J Control Rel 2005;104:477–88.
[14] Huynh DP, Shim WS, Kim JH, Lee DS. Polymer 2006;47:7918–26.
[15] Ju HK, Kim SY, Lee YM. Polymer 2001;42:6851–7.
[16] Schild HG. Prog Polym Sci 1992;17:163–249.
[17] Nguyen MK, Park DK, Lee DS. Biomacromolecules 2009;10:726–31.
[18] Kretlow JD, Hacker MC, Klouda L, Ma BB, Mikos AG. Biomacromolecules 2010;11:797–805.
[19] Zhang X, Li J, Li W, Zhang A. Biomacromolecules 2007;8:3557–67.
[20] He C, Zhao C, Chen X, Guo Z, Zhuang X, Jing X. Macromol Rapid Commun 2008;29:490–7.
[21] Zhao C, Zhuang X, He C, Chen X, Jing X. Macromol Rapid Commun 2008;29:1810–6.
[22] Lee RS, Li HR, Chiu FC. J Appl Polym Sci 2010;115:2556–64.
[23] Duan J, Du J, Zheng Y. J Appl Polym Sci 2007;103:3585–90.
[24] Lee RS, Yang JM, Huang KH. Polym J 1999;31:569–73.
[25] Choi SQ, Chae SY, Nah JW. Polymer 2006;47:4571–80.
[26] Nakayama M, Okano T, Miyazaki T, Kohori F, Sakai K, Yokoyama M. J Control Rel 2006;115:46–56.
[27] Chang C, Wei H, Quan CY, Li YY, Wang ZC, Cheng SX, et al. J Polym Sci Part A Polym Chem 2008;46:3048–57.
[28] Provencher SW, Hendrix J. J Phys Chem 1978;69:4237–76.
[29] Wilhelm M, Zhao CL, Wang Y, Xu R, Winnik A. Macromolecules 1991;24:1033–40.
[30] Shim IG, Kim SY, Lee YM, Cho CS, Sung YK. J Control Rel 1998;51:1–11.
[31] Lee RS, Chen WH. Polym Int, in press, doi:10.1002/pi.2937.